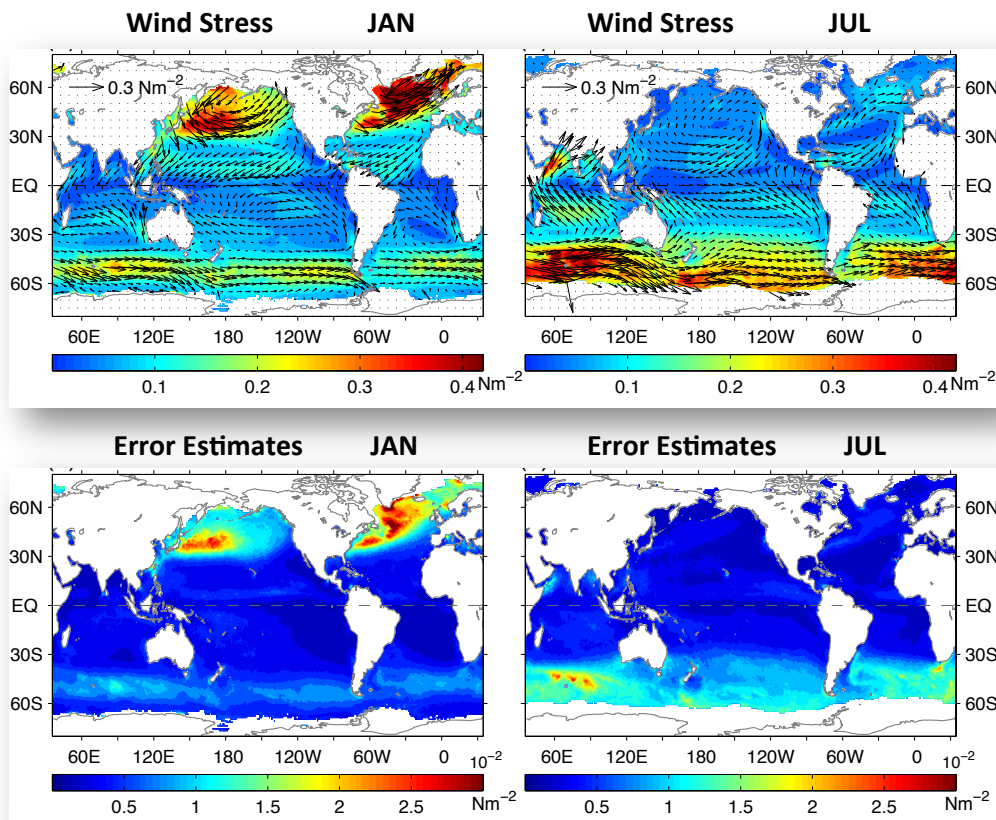




OAFlux High-Resolution Ocean-Surface Vector Wind Analysis Synergized from Satellite Scattermeters and Radiometers.

Part IV: Climatology of Surface Vector Wind, Wind Stress, and Derivatives with Uncertainty Estimates

Lisan Yu & Xiangze Jin



OAFlux Project Technical Report No. OA-2013-04
November 2013

Preface

A high-resolution global analysis of daily ocean-surface vector winds that covers the entire satellite wind observing period, from the first launch of SSMI in July 1987 to the present, was developed by the Objectively Analyzed air-sea Heat Fluxes (OAFlux) project. The OAFlux vector wind analysis is a synergy of 12 satellite sensors that includes 2 scatterometers (QuikSCAT and ASCAT) and 10 passive microwave radiometers (AMSRE, 6 SSMI sensors, and 2 SSMIS sensors, and the passive polarimetric microwave radiometer from WindSat).

A four-part report series is prepared, aiming to provide a systematic and conceptually organized review of the 12-sensor synergy and to support the public release of the datasets. Part I focuses on the methodology, approaches, and challenging technical issues in developing the multi-sensor synthesis. Part II documents the approach of error estimation that is developed to address the confidence and sensitivity of the OAFlux time series. Part III includes buoy-based validation. Part IV presents the OAFlux climatology of near-surface ocean vector winds and associated uncertainty estimates. The report series are developed from three research papers that were produced during the course of data development.

The datasets are freely available to interested users for non-commercial scientific research. For further information, please visit the project website at <http://oaflux.whoi.edu/> or contact the project PI (lyu@whoi.edu). The project is sponsored by the NASA Ocean Vector Wind Science Team (OVWST) activities. We sincerely thank the NASA support and technical input given by the international OVWST community during the four-year development.

Project PI: Lisan Yu
Woods Hole Oceanographic Institution

Abstract

This report is the fourth part of the four-part report series, presenting the OAFlux climatology of the near-surface vector wind, wind stress, wind and wind stress derivative fields and the associated uncertainty estimates for wind and wind stress components. The climatology represents the 25-year mean average of the OAFlux analysis from 1988 to 2012.

Wind speed, zonal and meridional wind components are the independent variables that are produced by the OAFlux 12-sensor synthesis. The wind stress, and zonal and meridional stress components are computed from the most recent COARE bulk flux algorithm version 3.5. We thank Jim Edson and Chris Fairall for providing the COARE version 3.5 codes and advice during the computation of wind stress.

Key words: remote sensing, climate record of ocean-surface vector wind, scatterometer, passive microwave radiometer, mesoscale air-sea interaction

Table of Contents

Preface	2
Abstract	3
1. Introduction	7
2. Climatological fields	8
2.1 Wind speed, zonal and meridional wind components with uncertainty estimates	8
2.2 Wind stress, zonal and meridional wind stress components with uncertainty estimates... 8	
2.3 Wind and wind stress derivative fields	10
3. Summary	10
Acknowledgements	10
References	11
Appendix: Differences between COARE v3.5 and v3.0 wind stress fields	12
Figure Captions	13
Figure 1. Wind speed and wind vector averaged over the period 1988-2012 for (a) January, (b) July, (c) annual mean, and (d) seasonal standard deviation (STD).	16
Figure 2. Zonal wind component averaged during 1988-2012 for (a) January, (b) July, (c) annual mean, and (d) STD.	17
Figure 3. Meridional wind component averaged during 1988-2012 for (a) January, (b) July, (c) annual mean, and (d) STD.	18
Figure 4. Zonally averaged (a) wind speed, (b) zonal wind component, and (c) meridional wind component during 1988-2012 for January, July, and annual mean.	19
Figure 5. Uncertainty estimates for wind speed for (a) January, (b) July, and (c) annual mean averaged during 1988-2012.	20

Figure 6. Uncertainty estimates for zonal wind component for (a) January, (b) July, and (c) annual mean averaged during 1988-2012.	21
Figure 7. Uncertainty estimates for meridional wind component for (a) January, (b) July, and (c) annual mean averaged during 1988-2012.	22
Figure 8. Wind stress and stress vector averaged during 1988-2012 for (a) January, (b) July, (c) annual mean, and (d) STD.	23
Figure 9. Zonal wind stress component averaged during 1988-2012 for (a) January, (b) July, (c) annual mean, and (d) STD.	24
Figure 10. Meridional wind stress component averaged during 1988-2012 for (a) January, (b) July, (c) annual mean, and (d) STD.	25
Figure 11. Zonally averaged (a) wind stress, (b) zonal wind stress component, and (c) meridional wind stress component averaged during 1988-2012 for January, July, and annual mean.	26
Figure 12. Uncertainty estimates for wind stress for (a) January, (b) July, and (c) annual mean averaged during 1988-2012.	27
Figure 13. Uncertainty estimates for zonal wind stress for (a) January, (b) July, and (c) annual mean averaged during 1988-2012.	28
Figure 14. Uncertainty estimates for meridional wind stress for (a) January, (b) July, and (c) annual mean averaged during 1988-2012.	29
Figure 15. Wind stress curl averaged during 1988-2012 for (a) January, (b) July, (c) annual mean, and (d) STD. Positive (negative) values denote clockwise (counterclockwise) circulation.	30

Figure 16. Surface wind divergence averaged during 1988-2012 for (a) January, (b) July, (c) annual mean, and (d) STD. Positive (negative) values denote surface divergence (convergence).31

Figure 17. Zonally averaged (a) wind stress curl, and (b) surface wind divergence averaged during 1988-2012 for January, July, and annual mean.32

Figure 18. Wind stress computed from (a) COARE v3.5, (b) COARE v3.0. (c) the differences between (a) and (b), and (d) the percentage of the differences. The three-year (2010-2012) mean averages were used as an example.33

Figure 19. Wind stress curl computed from (a) COARE v3.5, (b) COARE v3.0, and (c) the differences between (a) and (b). The three-year (2010-2012) mean averages were used as an example.34

Figure 20. The bin-averaged drag coefficients versus wind speed where the error bars represent the standard deviation about the mean. The dashed line represents the COARE 3.0 algorithm, while the solid line is the COARE 3.5 algorithm. The dashed–dotted line is the function provided by Large and Pond (1981) (from Figure 6 in Edson et al. [2013]).35

Figure 21. Scatter plot of COARE v3.5 wind stresses (x-axis) versus COARE 3.0 wind stressed (y-axis). The plot was constructed from daily values from all ocean grid points in year 2010.36

Introduction

In the past four years, the Objectively Analyzed air-sea Heat Fluxes (OAFlux) project at the Woods Hole Oceanographic Institution (WHOI) has devoted efforts to develop a high-resolution (0.25-degree) global daily analysis of ocean-surface vector winds for the satellite period (July 1987 onwards) through synergizing 12 sensors including both scatterometers and passive microwave radiometers. A four-part technical report series was prepared, aiming to provide a systematic and conceptually organized review of the 12-sensor synergy and to support the public release of the datasets. This report is the fourth part of the report series, presenting the OAFlux climatology of the near-surface vector wind, wind stress, wind and wind stress derivative fields and the associated uncertainty estimates for wind and wind stress components. The climatology represents the 25-year mean average of the OAFlux analysis from 1988 to 2012. The methodology, approaches, and challenging issues in developing the multi-sensor OAFlux synthesis are included in Part I [Yu and Jin 2013a], while the quantification of the sensitivity of the OAFlux time series to intersensor differences at high winds and heavy rainfall conditions and the confidence of the synthesis are in Part II [Yu and Jin 2013b]. The third part reports the evaluation of the OAFlux wind products using surface wind time series measurements from 126 moored buoys [Yu and Jin 2012].

The OAFlux project is a research project, with central foci on air-sea exchanges of heat, moisture, and momentum and their role in global climate variability and change. The OAFlux has distributed global time series of ocean evaporation, air-sea latent and sensible heat fluxes, and flux-related surface meteorological variables from 1958 onward with a near real-time update (<http://oaflux.whoi.edu>). This new 25-year analysis of ocean surface vector wind extends

OAFflux existing surface flux data base, making it a site of choice for consistent, quality, multidecadal time series of air-sea heat, moisture, and momentum fluxes.

2. Climatological fields

2.1 Wind speed, zonal and meridional wind components with uncertainty estimates

The OAFflux winds were calibrated as the equivalent neutral stability winds at a height of 10 m. Wind speed, zonal and meridional wind components are the independent variables that are produced by the OAFflux 12-sensor synthesis [e.g. Eq.(1) in the technical report Part I], and the climatological fields of the three variables in January, July, annual mean, and the standard deviation of the monthly mean are shown in Figures 1-3, respectively, with zonally averaged means summarized in Figure 4. The associated uncertainty estimates for wind speed and components are shown in Figures 5-7, respectively. The uncertainty estimates were computed from Eqs.(4)-(6) in the technical report Part II and represent the ensemble standard deviations of the posteriori diagnostics with 40 different sets of weights.

The mean global surface wind pattern features trade winds in the tropical oceans and westerlies in mid latitudes between 30-60° north and south. Despite the differences in the mean patterns, the uncertainty estimates of the three variable have a similar pattern albeit with different magnitude. Large uncertainties are associated with the tropical rain bands (e.g., ITCZ and SPCZ) and the mid-latitude storm track regions, due to the technical difficulties of satellite retrievals in rain and high wind conditions [Yu and Jin, 2013a&b].

2.2 Wind stress, zonal and meridional wind stress components with uncertainty estimates

The wind stress, τ , and zonal and meridional stress components, τ_x and τ_y , are computed from the bulk formula:

$$\tau = \rho C_d w^2 \quad (1a)$$

$$\tau_x = \rho C_d w u \quad (1b)$$

$$\tau_y = \rho C_d w v \quad (1c)$$

where ρ is the density of air, C_d drag coefficient. The bulk flux algorithm that the OAFlex wind stress was used is the newly refined COARE version 3.5 [Edison *et al.* 2013; hereafter v3.5]. The differences in wind stress fields due to the differences in the COARE version 3.0 [Fairall *et al.* 2003; hereafter v3.0] and v3.5 are included in Appendix A.

The climatological fields of wind stress magnitude, zonal and meridional stress components in January, July, annual mean, and the standard deviation of the monthly mean are shown in Figures 9-10, respectively, with zonally averaged means summarized in Figure 11. The associated uncertainty estimates for the three variables were computed from Eqs. (4)-(6) in the technical report Part II and are shown in Figures 12-14, respectively.

Like the wind and wind components, the stress and stress components also display a similar uncertainty pattern. However, unlike the wind and wind components that have considerable uncertainties both in the tropical rain belts and in the mid-latitude storm track regions, the stress and stress components show significant uncertainties mostly in the mid latitudes. As shown in Eqs. (9)-(12), the uncertainty estimation for wind stress and components is the propagation of the uncertainties of wind and wind components with Therefore, the uncertainties in wind stress and stress components have a greater dependence of the magnitude of wind speed. The winds in the storm track regions are gusty, and so the uncertainty in winds a larger uncertainty in wind stress.

2.3 Wind and wind stress derivative fields

Wind stress curl is computed according to the following expression:

$$Curl(\tau) = \frac{\partial \tau_y}{\partial x} - \frac{\partial \tau_x}{\partial y} \quad (2)$$

Wind divergence is computed using the following expression:

$$div = \frac{\partial u}{\partial x} + \frac{\partial v}{\partial y} \quad (3)$$

Figures 15 and 16 are the respective climatological fields for wind stress curl and wind divergence in January, July, annual mean, and monthly standard deviations. The zonally averages values are included in Figure 17.

3. Summary

A four-part technical report series was prepared, aiming to provide a systematic and conceptually organized review of the 12-sensor synergy and to support the public release of the datasets. This report is the fourth part of the report series, presenting the OAFlux climatology of the near-surface vector wind, wind stress, wind and wind stress derivative fields and the associated uncertainty estimates for wind and wind stress components. The climatology represents the 25-year mean average of the OAFlux analysis from 1988 to 2012.

Acknowledgements

The project is sponsored by the NASA Ocean Vector Wind Science Team (OVWST) activities under grant NNA10AO86G. We thank Jim Edson and Chris Fairall for providing the COARE version 3.5 codes and advice during the computation of wind stress.

References

- Edson, J. B., V. Jampana, R. A. Weller, S. Bigorre, A. J. Plueddemann, C. W. Fairall, S. D. Miller, L. Mahrt, D. Vickers, and H. Hersbach, (2013), On the exchange of momentum over the open ocean, *J. Phys. Oceanogr.*, **43**, 1589-1610.
- Fairall, C. W., E. F. Bradley, J. E. Hare, A. A. Grachev, and J. B. Edson, (2003), Bulk parameterization of air-sea fluxes: updates and verification for the coare algorithm. *J. Climate*, **19**, 571–591.
- Yu, L., and X. Jin, (2012), Buoy perspective of a high-resolution global ocean vector wind analysis constructed from passive radiometers and active scatterometers (1987-present). *J. Geophys. Res.*, **117**, C11013, doi:10.1029/2012JC008069.
- Yu, L. and X. Jin, (2013a): A Satellite-Derived High-Resolution Ocean Surface Vector Wind Analysis (1987 onward). Part I: Methodology, Approach, and Challenging issues. WHOI OAFlux project Technical Report, OA-2013-01, Woods Hole, Massachusetts. 72pp.
- Yu, L., and X. Jin, (2013b): A Satellite-Derived High-Resolution Ocean Surface Vector Wind Analysis (1987 onwards). Part II: Uncertainty estimation. WHOI OAFlux project Technical Report, OA-2013-02, Woods Hole, Massachusetts. 50pp.
- Yu, L., and X. Jin, (2013c): A Satellite-Derived High-Resolution Ocean Surface Vector Wind Analysis (1987 onwards). Part III: Buoy validation. WHOI OAFlux project Technical Report, OA-2013-03, Woods Hole, Massachusetts. 78pp.

Appendix: Differences between COARE v3.5 and v3.0 wind stress fields

The OAFlux wind stress computation takes advantage of the recent release of the COARE flux bulk algorithm version 3.5 [Edson *et al.* 2013]. To see the differences between the new COARE v3.5 and the previous version COARE v3.0 [Fairall *et al.*, 2003], we compared the wind stress computed from the two versions using a three year period 2010-2012 (Figs. 18a-d). It can be seen that COARE v3.5 produces stronger wind stress at higher latitudes and slightly weaker wind stress at low latitudes (Fig. 18c). Compared to COARE v3.0, the percentage of the mean change is about 4-7% increase for high winds in mid- and higher latitudes and 4-7% decrease for low winds in low latitudes. The related changes in wind stress curl field due to the differences in the two algorithms are shown in Figs 19a-c.

As discussed in Edson *et al.* [2013], COARE v3.5 improves parameterizations of the surface roughness and drag coefficient of the surface stress in the bulk formulas. The COARE v3.0 is found to underestimate the observed surface stresses and Charnock coefficients at high winds and overestimate these values at low winds. The wind speed dependence of the Charnock coefficient α in the COARE algorithm is then modified to $\alpha = mU_{10N} + b$, where $m = 0.017\text{m}^{-1} \text{ s}$ and $b = - 0.005$. Edson *et al.* [2013] found that when combined with a parameterization for smooth flow, this formulation gives better agreement with the stress estimates from all of the field programs at all winds speeds with significant improvement for wind speeds over 13 m s^{-1} up to 25 m s^{-1} (Fig.20, from Edson *et al.*).

The relationship between daily-mean OAFlux wind stress computed from the two versions can be seen more clearly from the scatter plot in Fig. 21, which shows that COARE v3.5 wind stresses are stronger than those of COARE v3.0 for wind stresses over 0.4 Nm^{-2} .

Figure captions

Figure 1. Wind speed (w , color shadings) and wind vector (arrows) averaged over the period 1988-2012 for (a) January, (b) July, (c) annual mean, and (d) seasonal standard deviation (STD). Unit: ms^{-1} .

Figure 2. Zonal wind component (u) averaged over the period 1988-2012 for (a) January, (b) July, and (c) annual mean. Seasonal standard deviation (STD) of u is shown in (d). Unit: ms^{-1} .

Figure 3. Meridional wind component (v) averaged over the period 1988-2012 for (a) January, (b) July, (c) annual mean, and (d) seasonal standard deviation (STD). Unit: ms^{-1} .

Figure 4. Zonally averaged (a) wind speed (w), (b) zonal wind component (u), and (c) meridional wind component (v) over the period 1988-2012 for January (blue curve), July (red curve), and annual mean (black curve). Unit: ms^{-1} .

Figure 5. Uncertainty estimates for wind speed (w) for (a) January, (b) July, and (c) annual mean averaged over 1988-2012. Unit: ms^{-1} .

Figure 6. Uncertainty estimates for zonal wind component (u) for (a) January, (b) July, and (c) annual mean averaged over 1988-2012. Unit: ms^{-1} .

Figure 7. Uncertainty estimates for meridional wind component (v) for (a) January, (b) July, and (c) annual mean averaged over 1988-2012. Unit: ms^{-1} .

Figure 8. Wind stress (τ , color shadings) and stress vector (arrows) averaged over the period 1988-2012 for (a) January, (b) July, (c) annual mean, and (d) seasonal standard deviation (STD). Unit: Nm^{-2} .

Figure 9. Zonal wind stress component (τ_x) averaged over the period 1988-2012 for (a) January, (b) July, (c) annual mean, and (d) seasonal standard deviation (STD). Unit: Nm^{-2} .

Figure 10. Meridional wind stress component (τ_y) averaged over the period 1988-2012 for (a) January, (b) July, (c) annual mean, and (d) seasonal standard deviation (STD). Unit: Nm^{-2} .

Figure 11. Zonally averaged (a) wind stress (τ), (b) zonal wind stress component (τ_x), and (c) meridional wind stress component (τ_y) over the period 1988-2012 for January (blue curve), July (red curve), and annual mean (black curve). Unit: Nm^{-2} .

Figure 12. Uncertainty estimates for wind stress (τ) for (a) January, (b) July, and (c) annual mean averaged over 1988-2012. Unit: ms^{-1} .

Figure 13. Uncertainty estimates for zonal wind stress (τ_x) for (a) January, (b) July, and (c) annual mean averaged over 1988-2012. Unit: ms^{-1} .

Figure 14. Uncertainty estimates for meridional wind stress (τ_y) for (a) January, (b) July, and (c) annual mean averaged over 1988-2012. Unit: ms^{-1} .

Figure 15. Wind stress curl ($\text{curl}(\tau)$) averaged over the period 1988-2012 for (a) January, (b) July, (c) annual mean, and (d) seasonal standard deviation (STD). Unit: 10^{-7}Nm^{-3} . Positive (negative) values denote clockwise (counterclockwise) circulation.

Figure 16. Surface wind divergence (div) averaged over the period 1988-2012 for (a) January, (b) July, (c) annual mean, and (d) seasonal standard deviation (STD). Unit: 10^{-6}s^{-1} . Positive (negative) values denote surface divergence (convergence).

Figure 17. Zonally averaged (a) wind stress curl ($\text{curl}\tau$), and (b) surface wind divergence (div) over the period 1988-2012 for January (blue curve), July (red curve), and annual mean (black curve).

Figure 18. Wind stress computed from using (a) the most recent COARE v3.5, (b) COARE v3.0. (c) the differences between wind stress using v3.5 and those using v3.0, and (d) the percentage of the differences. The three-year (2010-2012) mean averages were used as an example.

Figure 19. Wind stress curl computed from (a) COARE v3.5, (b) COARE v3.0, and (c) the differences due to the differences in the two COARE versions. The three-year (2010-2012) mean averages were used as an example.

Figure 20. The bin-averaged drag coefficients versus wind speed where the error bars represent the standard deviation about the mean. The dashed line represents the COARE 3.0 algorithm, while the solid line is the COARE 3.5 algorithm. The dashed-dotted line is the function provided by Large and Pond (1981) (from Figure 6 in Edson et al. [2013]).

Figure 21. Scatter plot of COARE v3.5 wind stresses (x-axis) versus COARE 3.0 wind stressed (y-axis). The plot was constructed from daily values from all ocean grid points in year 2010.

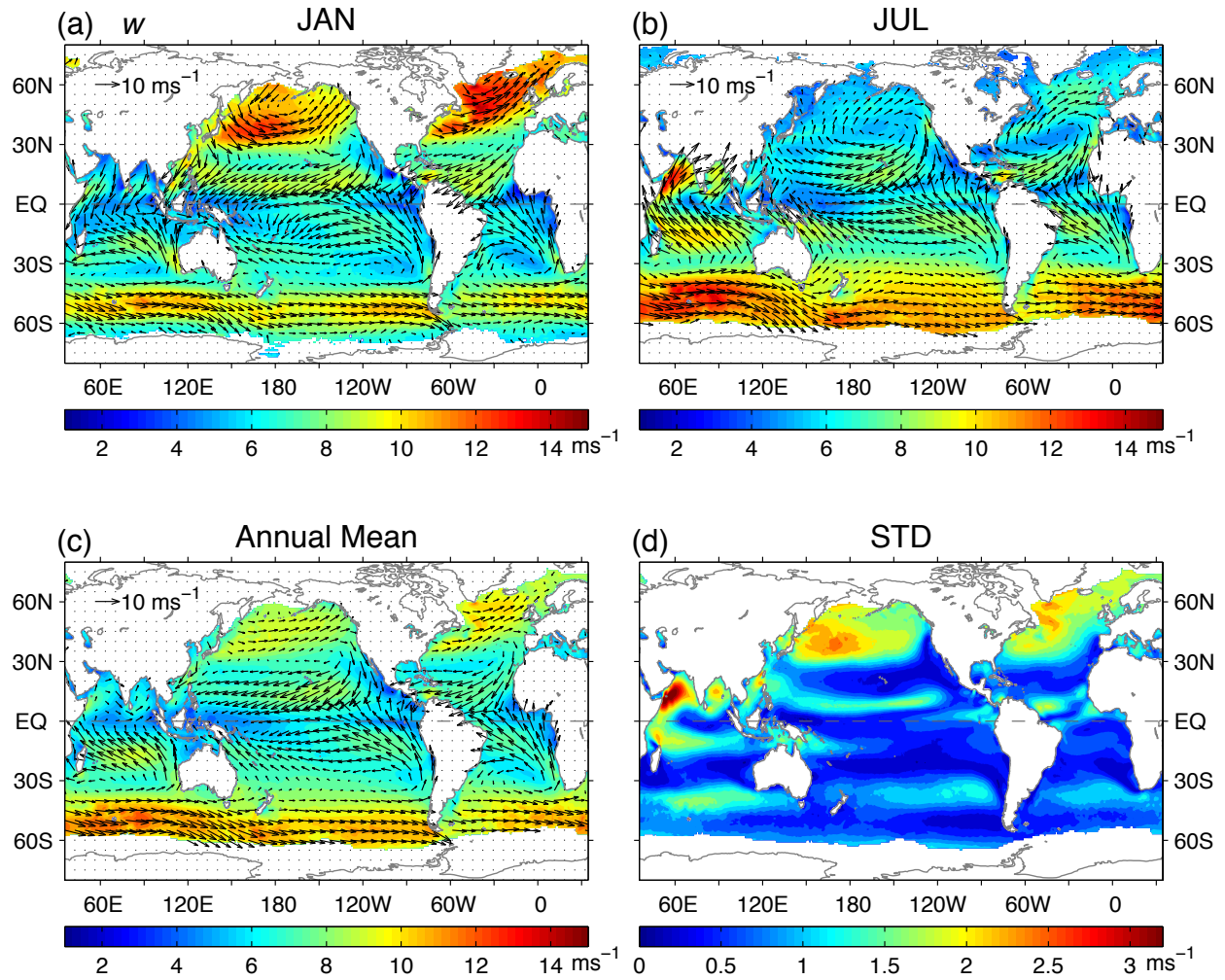


Figure 1. Wind speed (w , color shadings) and wind vector (arrows) averaged over the period 1988-2012 for (a) January, (b) July, (c) annual mean., and (d) seasonal standard deviation (STD). Unit: ms^{-1} .

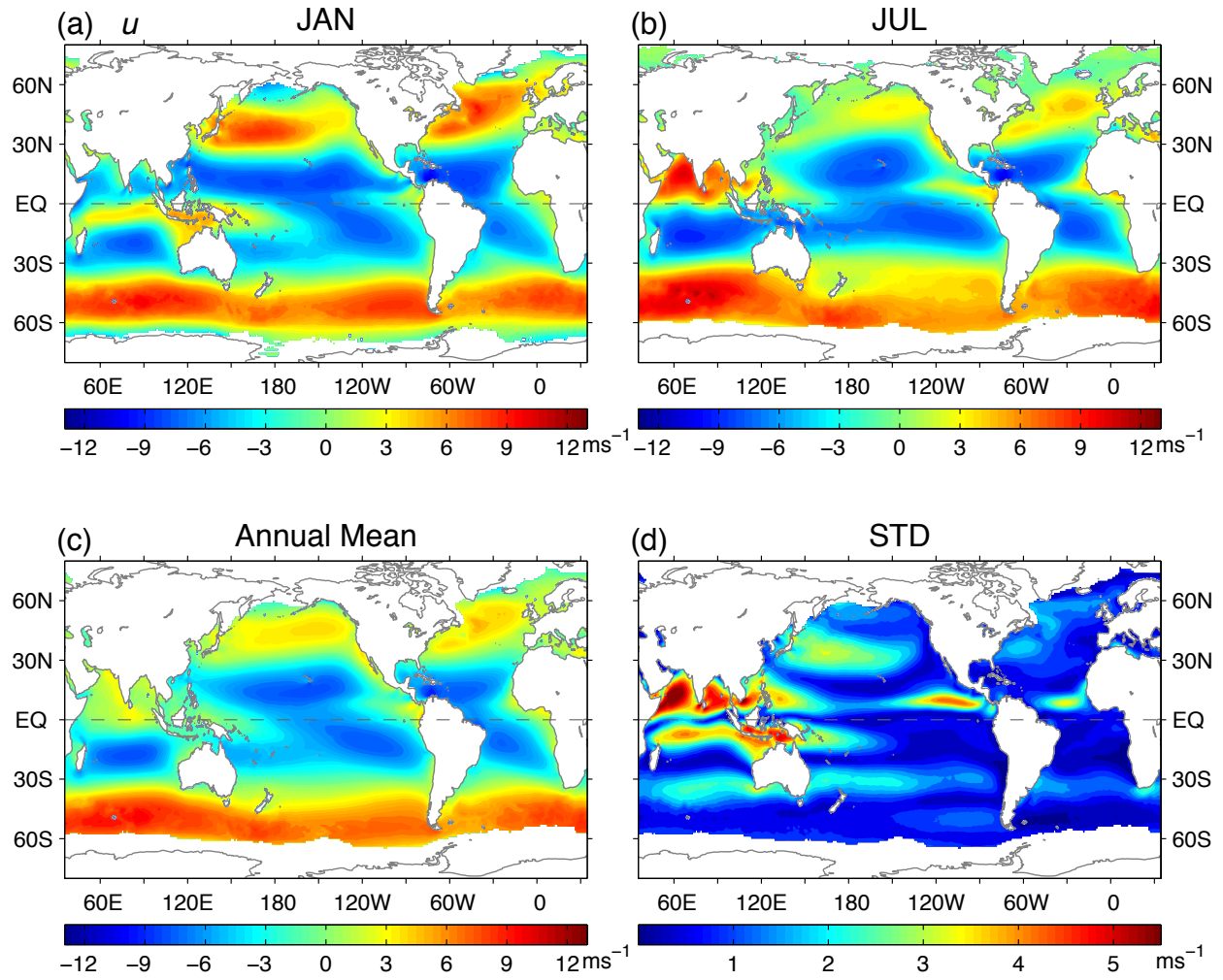


Figure 2. Zonal wind component (u) averaged over the period 1988-2012 for (a) January, (b) July, (c) annual mean, and (d) seasonal standard deviation (STD). Unit: ms^{-1} .

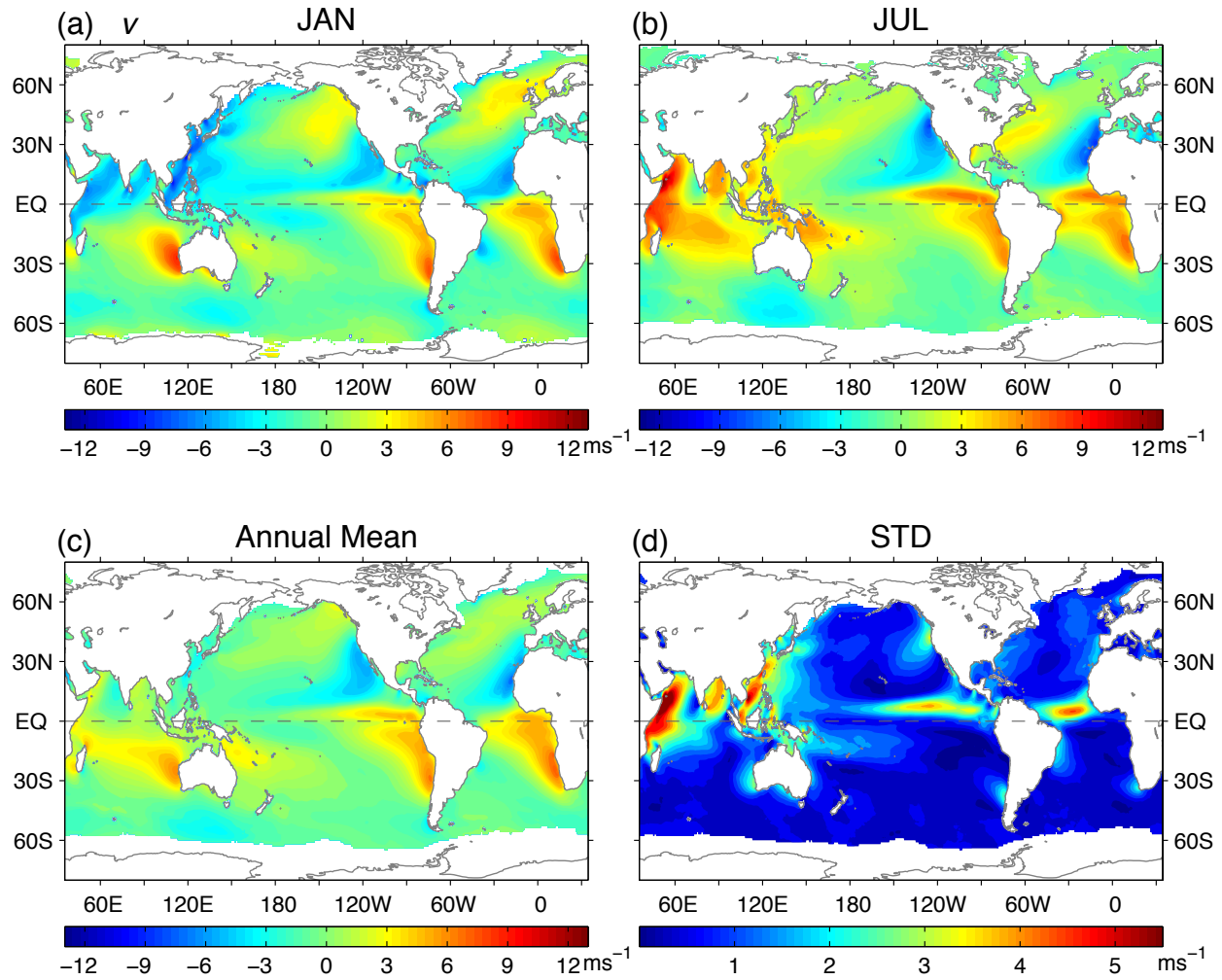


Figure 3. Meridional wind component (v) averaged over the period 1988-2012 for (a) January, (b) July, (c) annual mean, and (d) seasonal standard deviation (STD). Unit: ms^{-1} .

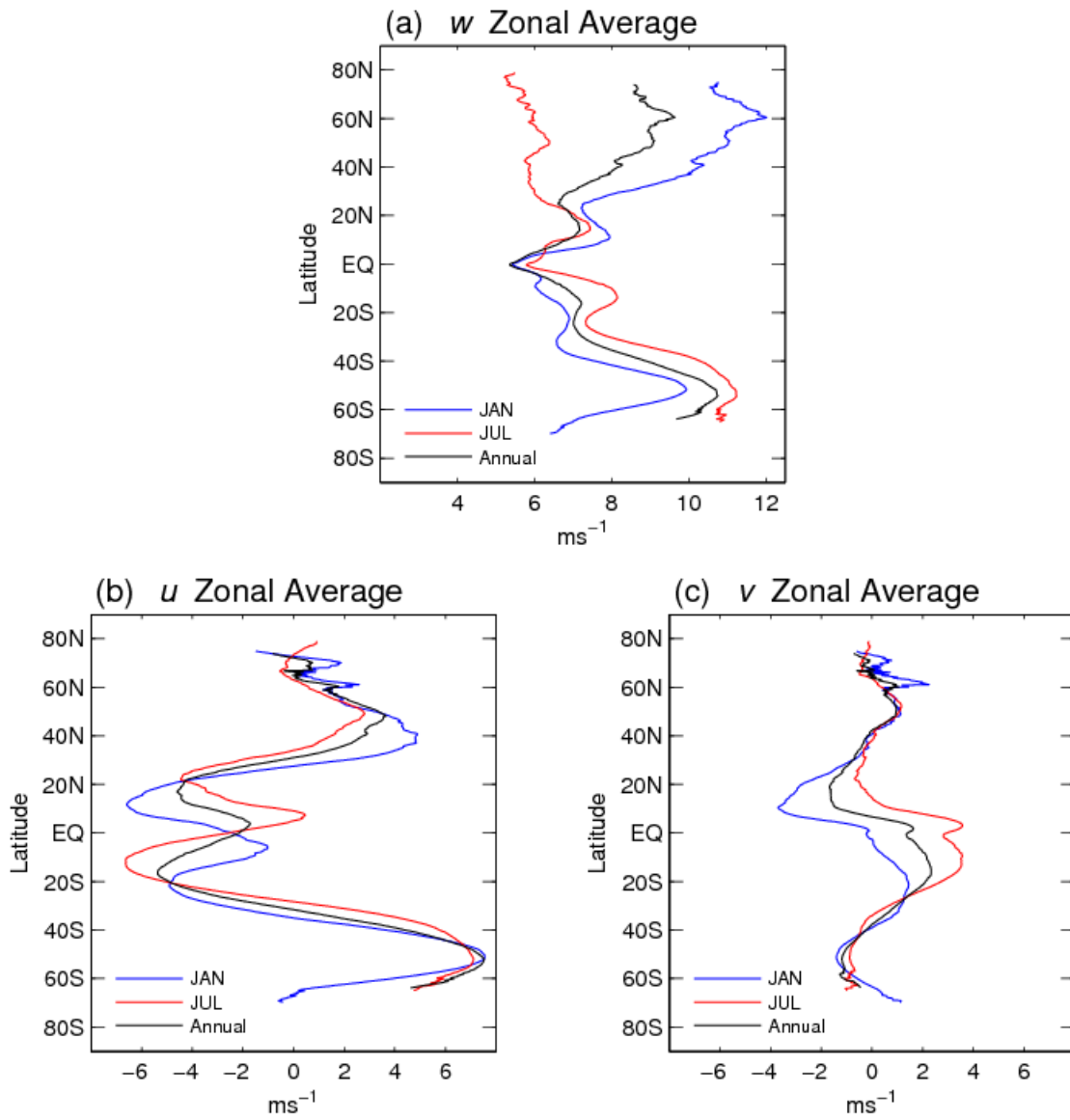


Figure 4. Zonally averaged (a) wind speed (w), (b) zonal wind component (u), and (c) meridional wind component (v) over the period 1988-2012 for January (blue curve), July (red curve), and annual mean (black curve). Unit: ms^{-1} .

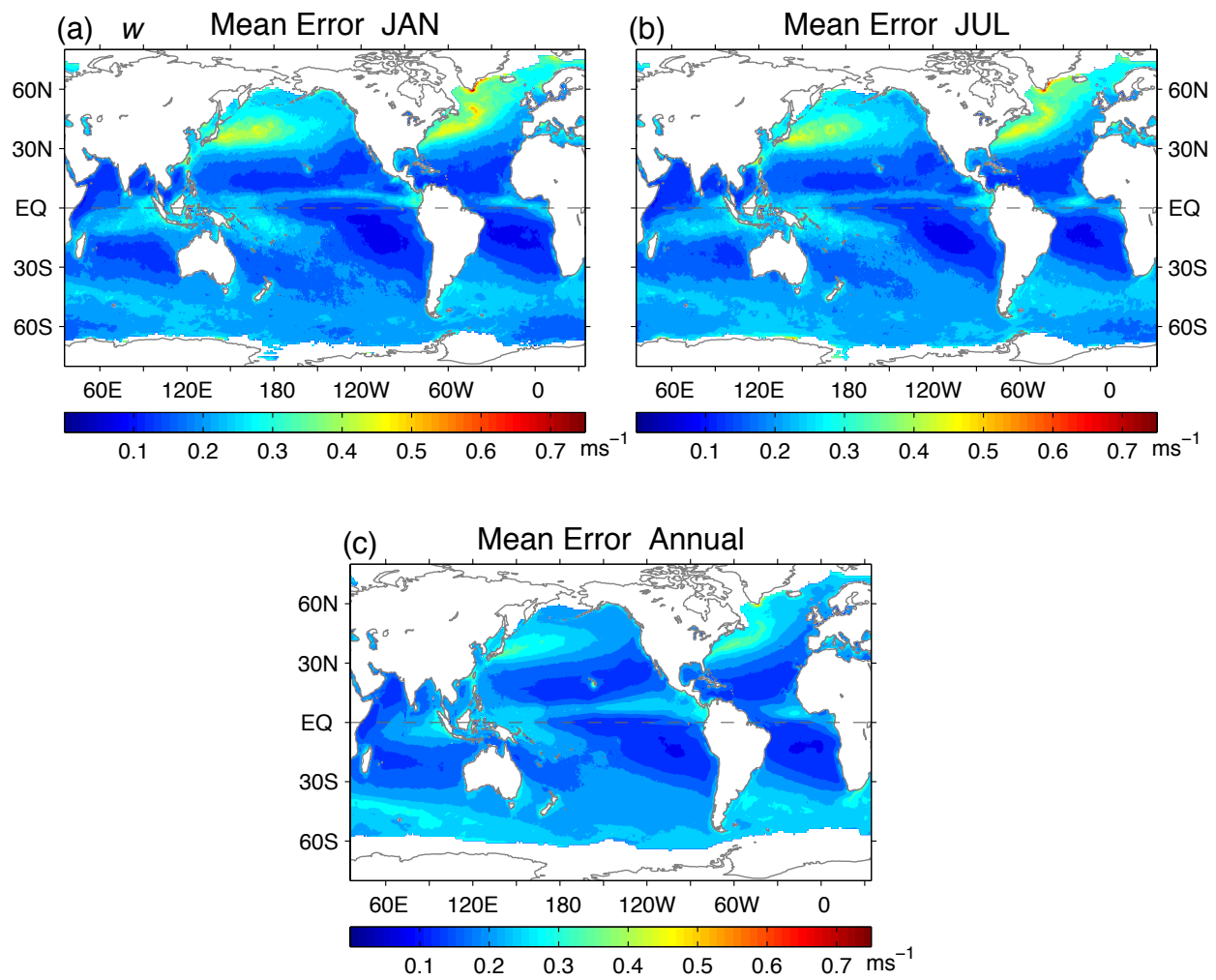


Figure 5. Uncertainty estimates for wind speed (w) for (a) January, (b) July, and (c) annual mean averaged over 1988-2012. Unit: ms^{-1} .

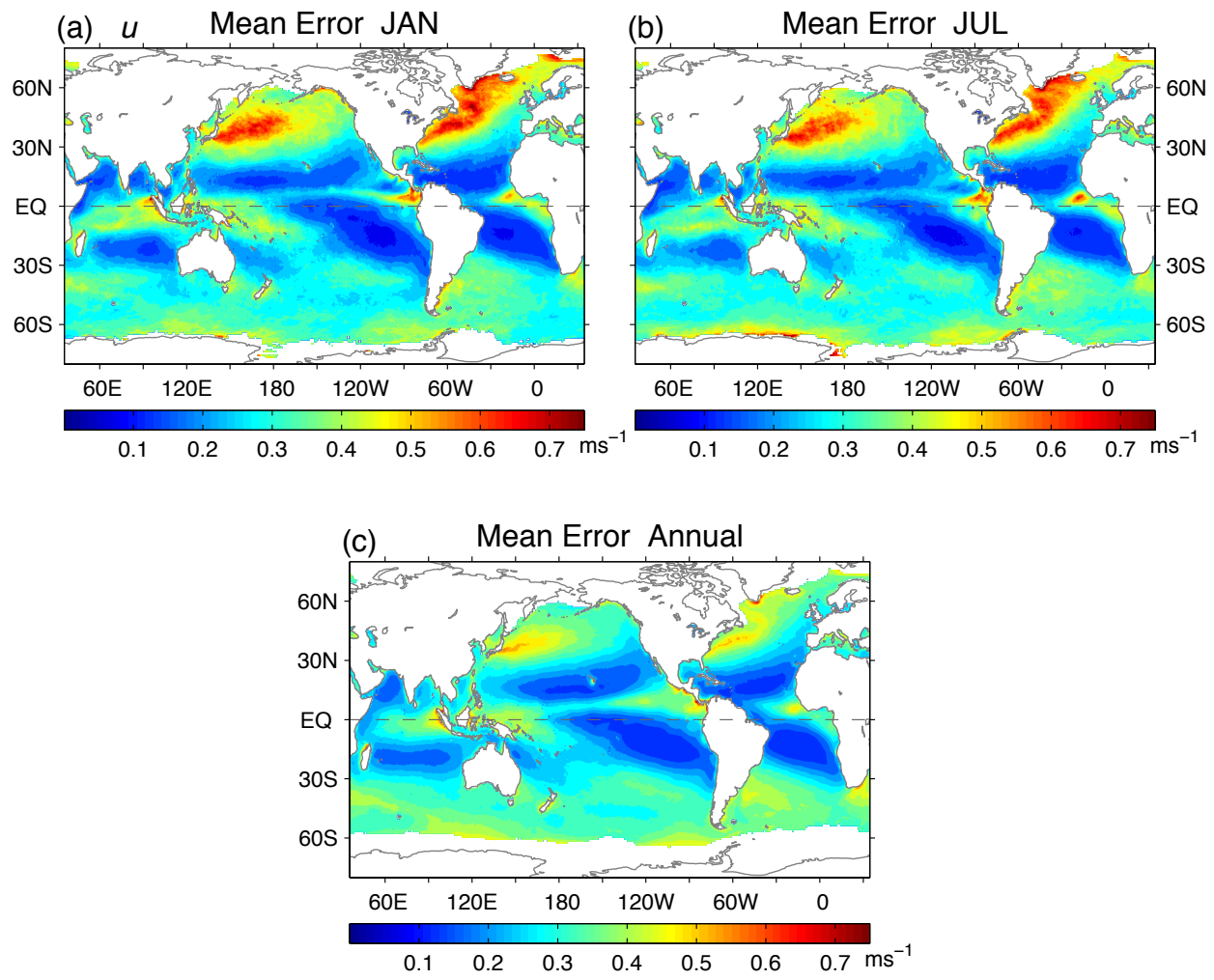


Figure 6. Uncertainty estimates for zonal wind component (u) for (a) January, (b) July, and (c) annual mean averaged over 1988-2012. Unit: ms^{-1} .

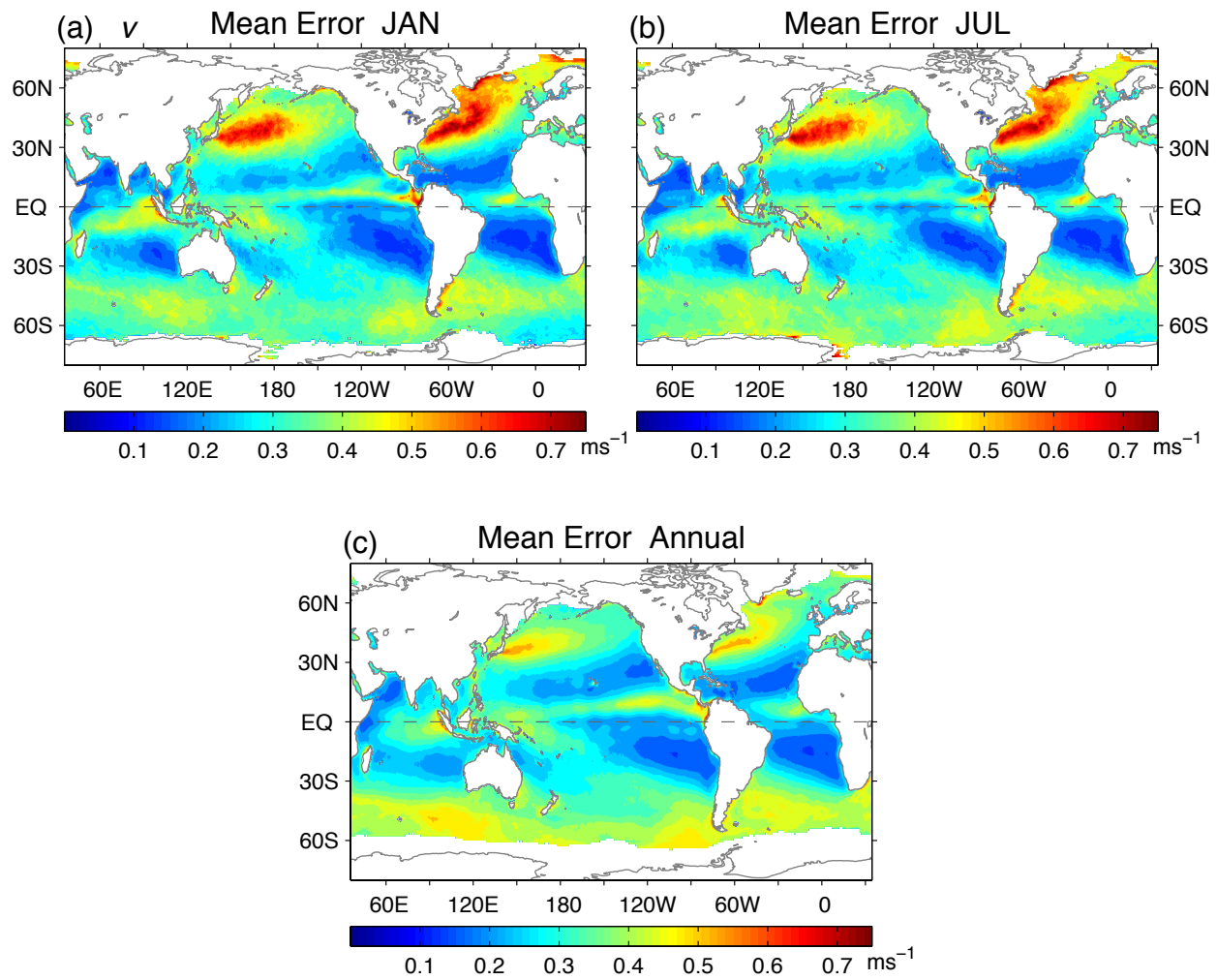


Figure 7. Uncertainty estimates for meridional wind component (v) for (a) January, (b) July, and (c) annual mean averaged over 1988-2012. Unit: ms^{-1} .

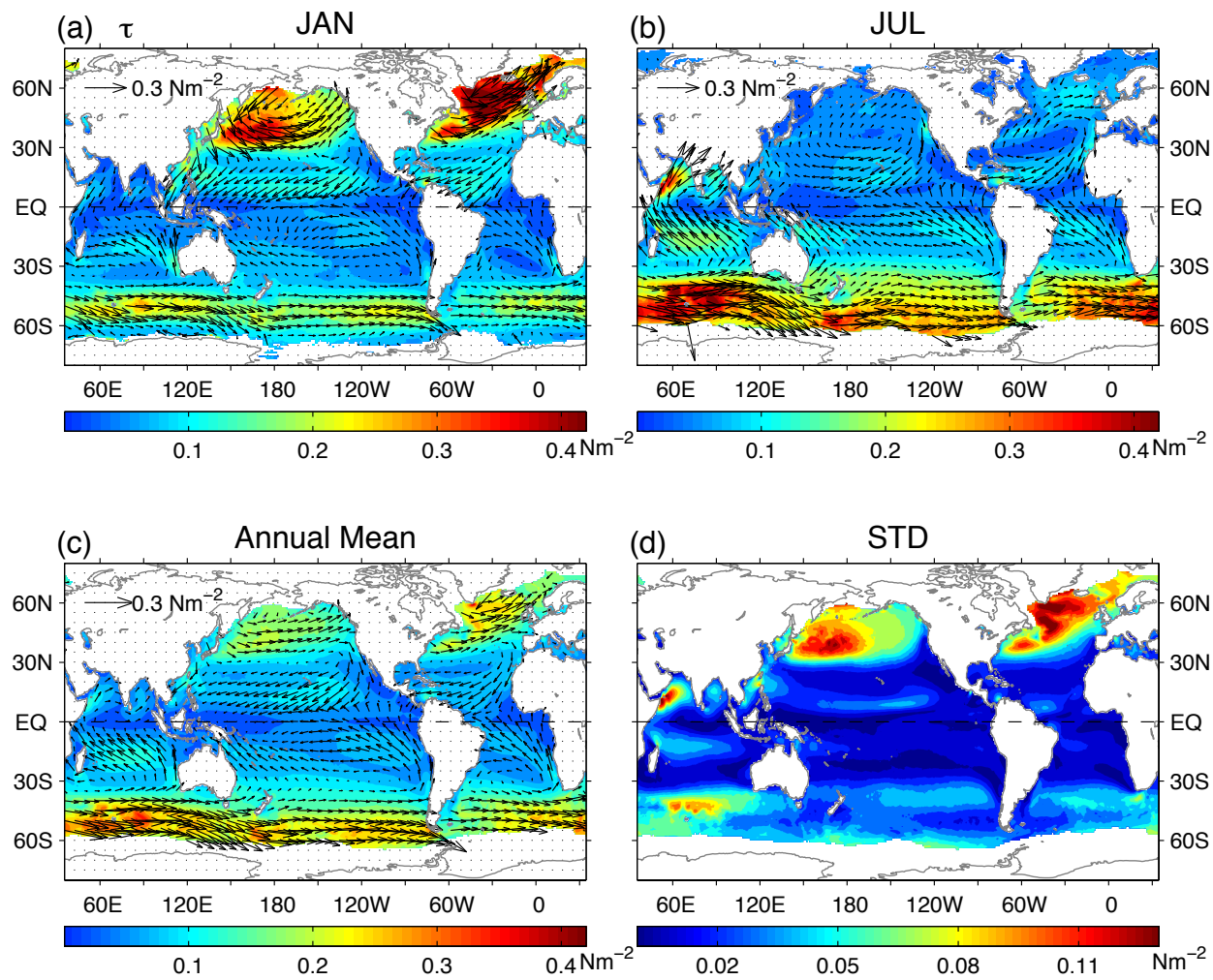


Figure 8. Wind stress (τ , color shadings) and stress vector (arrows) averaged over the period 1988-2012 for (a) January, (b) July, (c) annual mean, and (d) seasonal standard deviation (STD). Unit: Nm^{-2} .

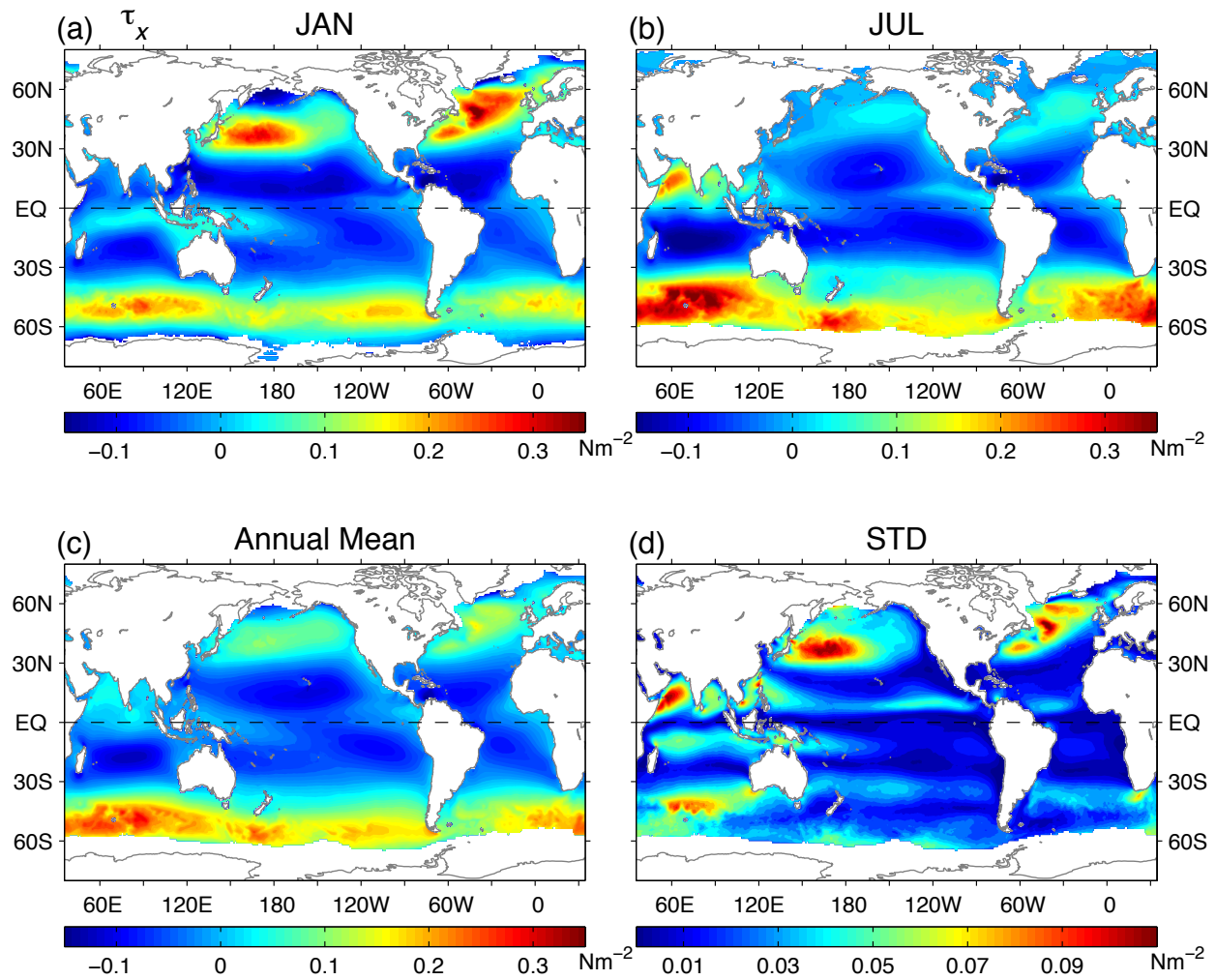


Figure 9. Zonal wind stress component (τ_x) averaged over the period 1988-2012 for (a) January, (b) July, (c) annual mean, and (d) seasonal standard deviation (STD). Unit: Nm^{-2} .

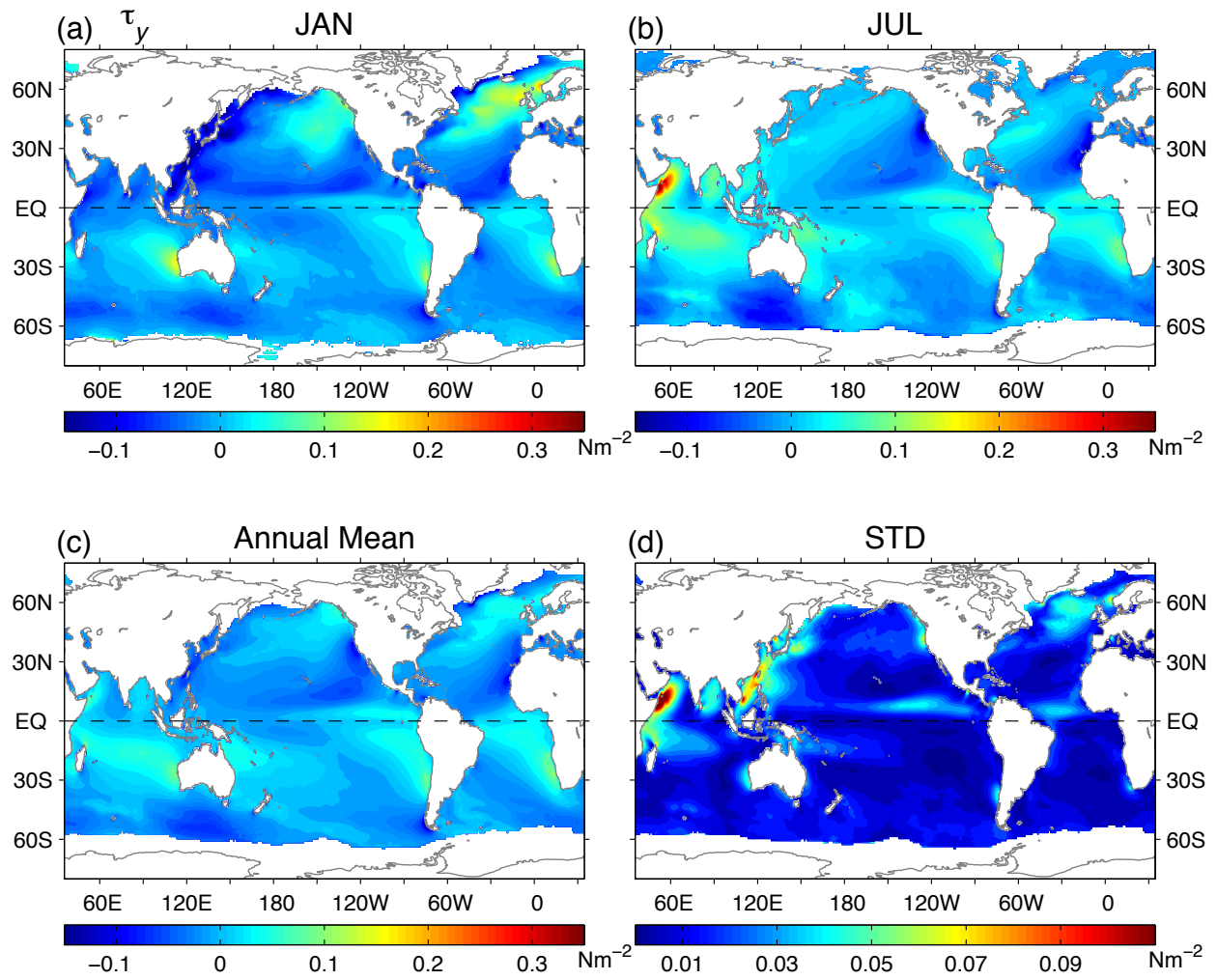


Figure 10. Meridional wind stress component (τ_y) averaged over the period 1988-2012 for (a) January, (b) July, (c) annual mean, and (d) seasonal standard deviation (STD). Unit: Nm^{-2} .

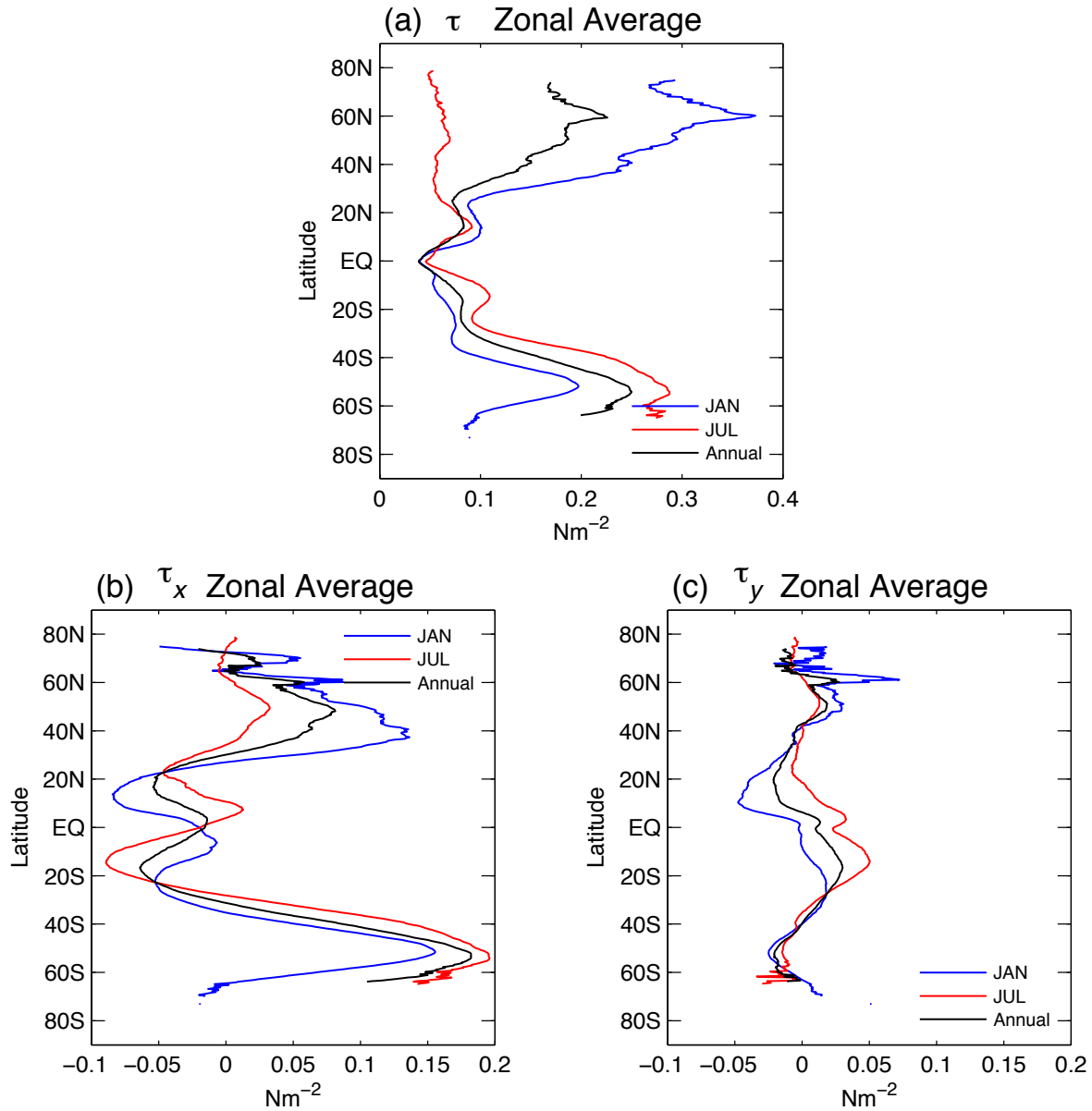


Figure 11. Zonally averaged (a) wind stress (τ), (b) zonal wind stress component (τ_x), and (c) meridional wind stress component (τ_y) over the period 1988-2012 for January (blue curve), July (red curve), and annual mean (black curve). Unit: Nm^{-2} .

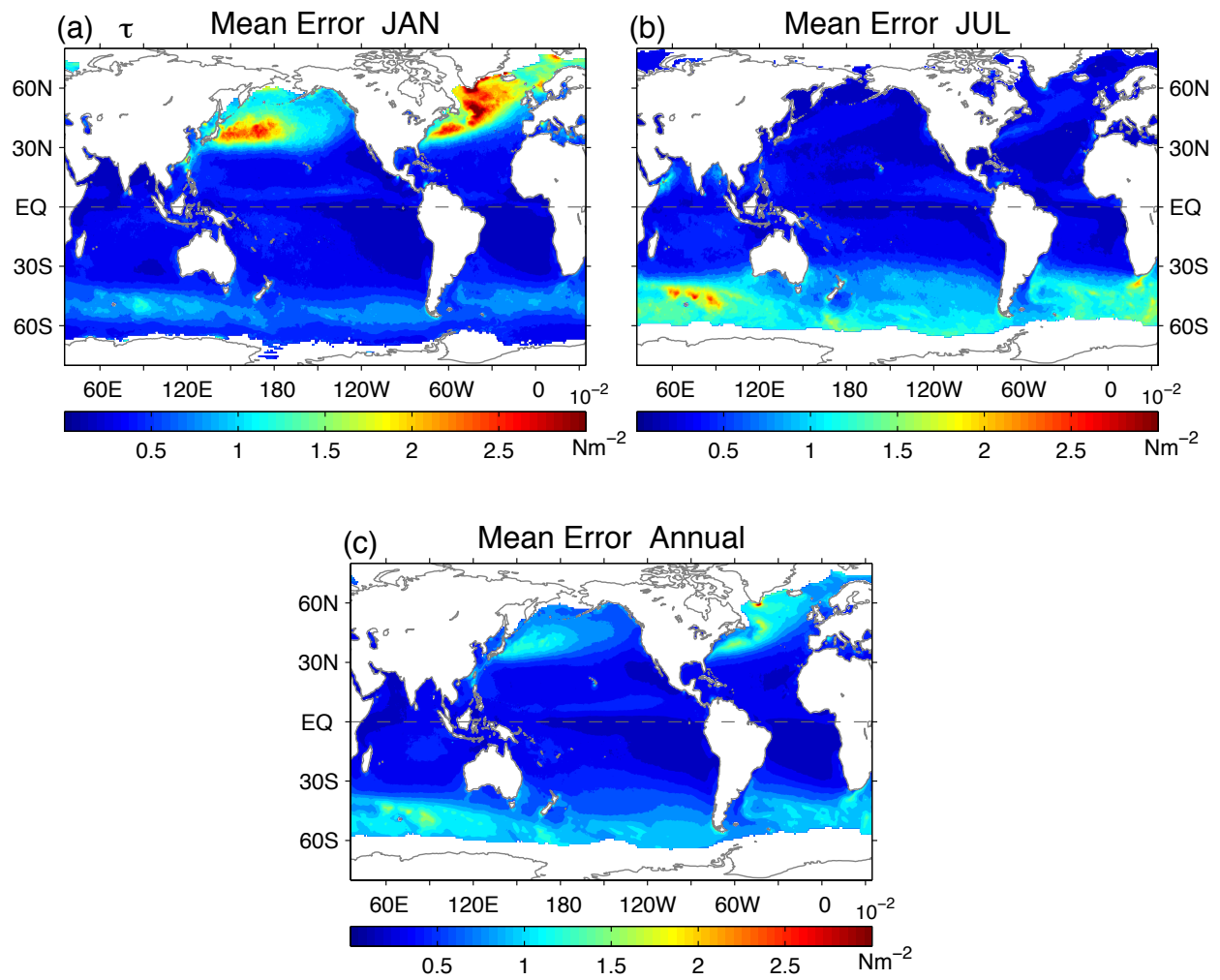


Figure 12. Uncertainty estimates for wind stress (τ) for (a) January, (b) July, and (c) annual mean averaged over 1988-2012. Unit: ms^{-1} .

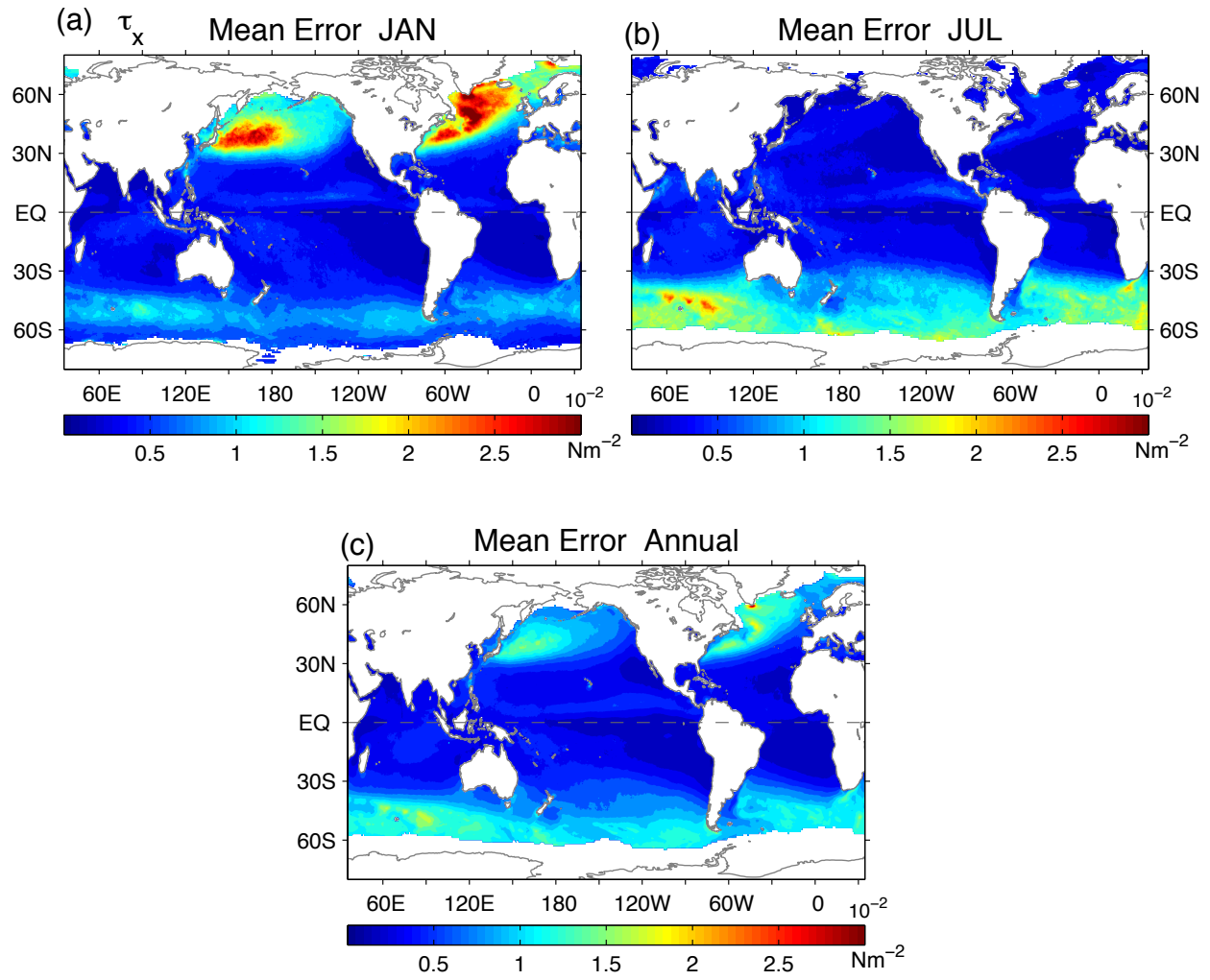


Figure 13. Uncertainty estimates for zonal wind stress (τ_x) for (a) January, (b) July, and (c) annual mean averaged over 1988-2012. Unit: ms^{-1} .

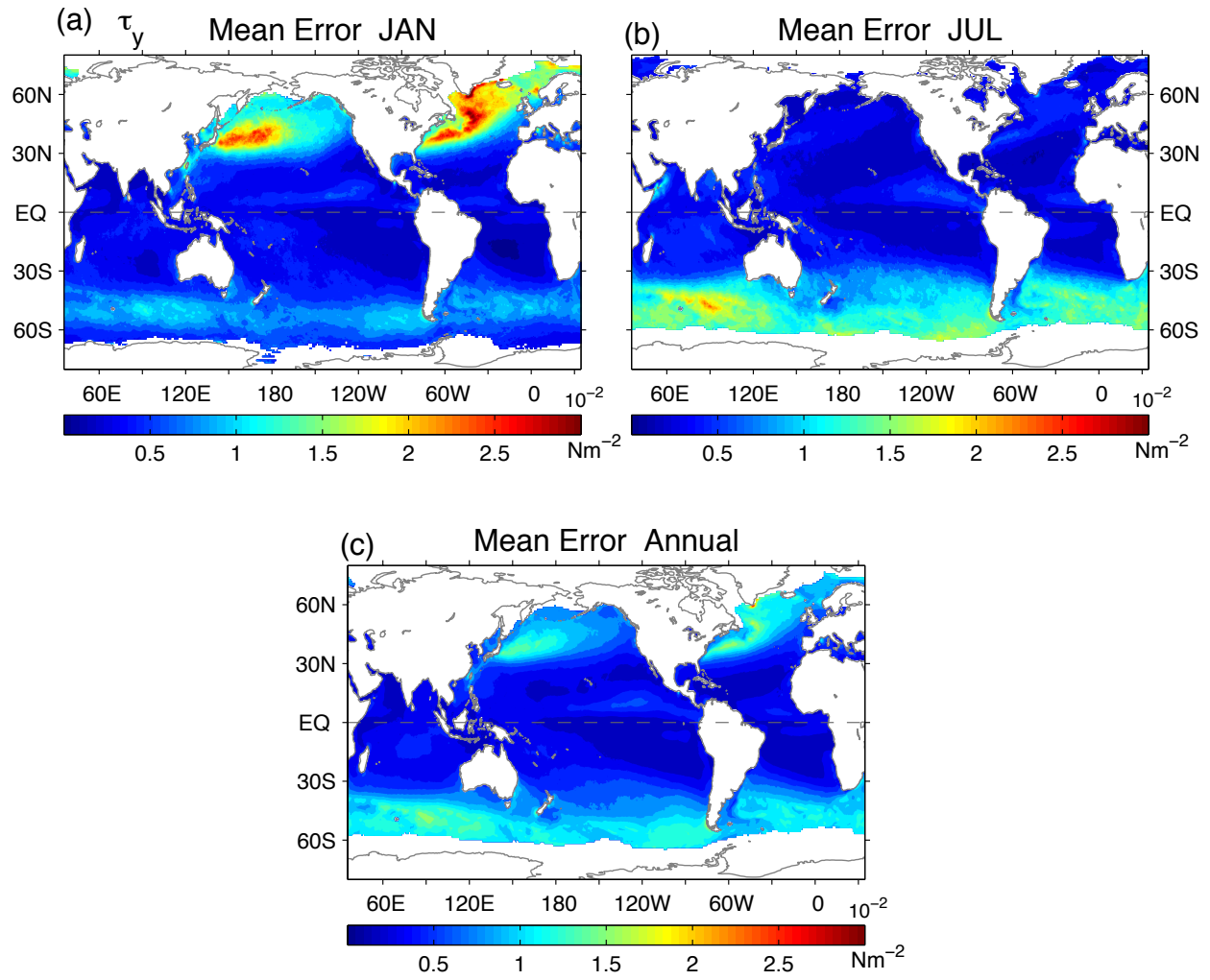


Figure 14. Uncertainty estimates for meridional wind stress (τ_y) for (a) January, (b) July, and (c) annual mean averaged over 1988-2012. Unit: ms^{-1} .

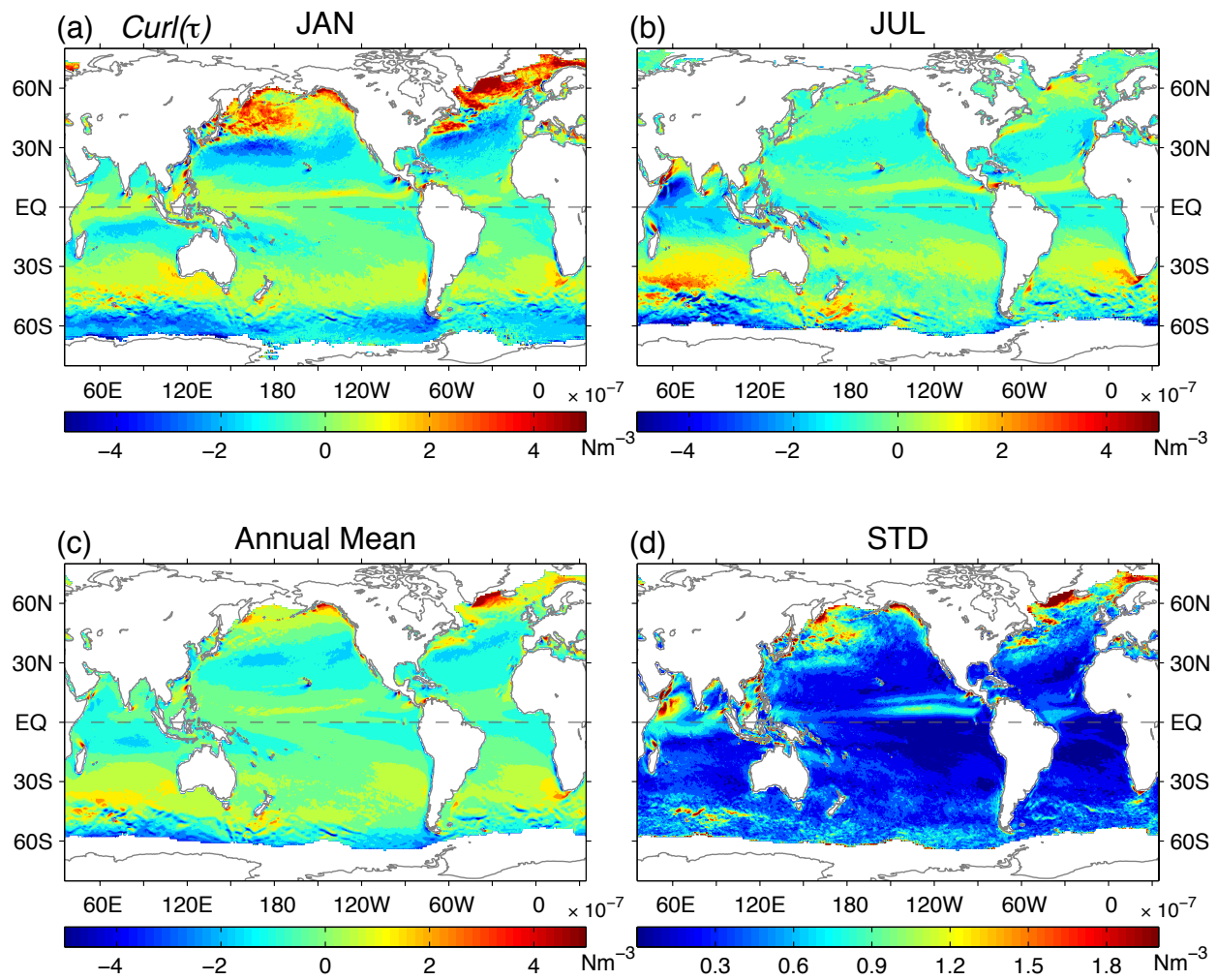


Figure 15. Wind stress curl ($curl(\tau)$) averaged over the period 1988-2012 for (a) January, (b) July, and (c) annual mean. Seasonal standard deviation (STD) of $curl(\tau)$ is shown in (d). Unit: 10^{-7} Nm^{-3} . Positive (negative) values denote clockwise (counterclockwise) circulation.

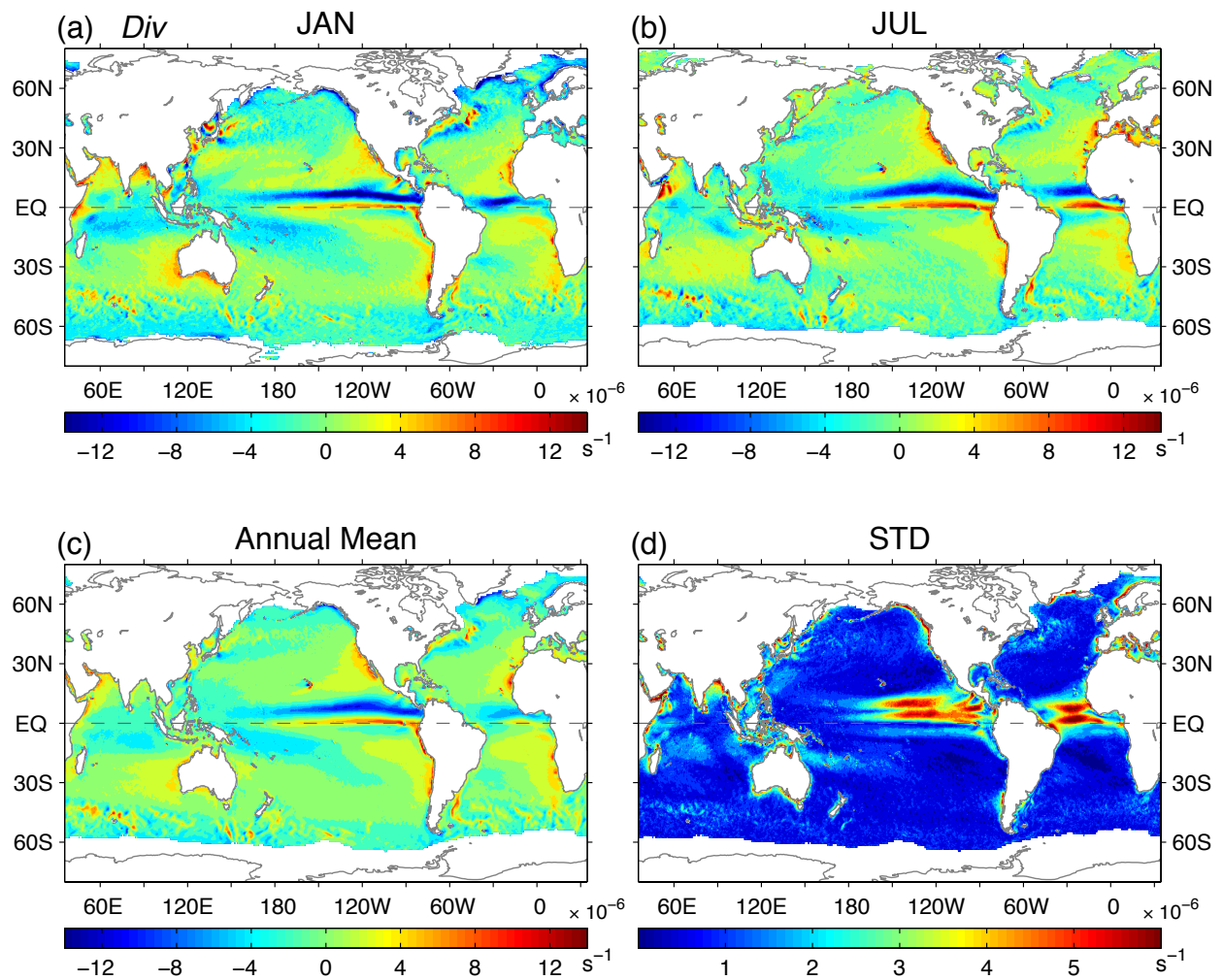


Figure 16. Surface wind divergence (*div*) averaged over the period 1988-2012 for (a) January, (b) July, (c) annual mean, and (d) seasonal standard deviation (STD). Unit: 10^{-6} s^{-1} . Positive (negative) values denote surface divergence (convergence).

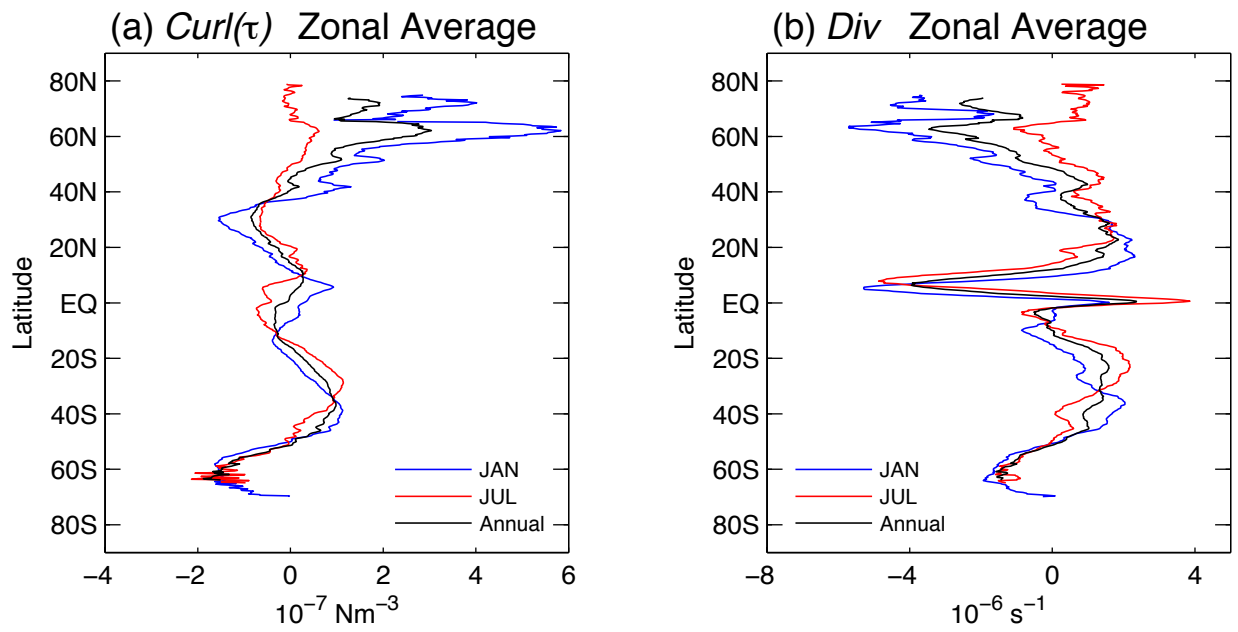


Figure 17. Zonally averaged (a) wind stress curl ($\text{curl}\tau$), and (b) surface wind divergence (div) over the period 1988-2012 for January (blue curve), July (red curve), and annual mean (black curve).

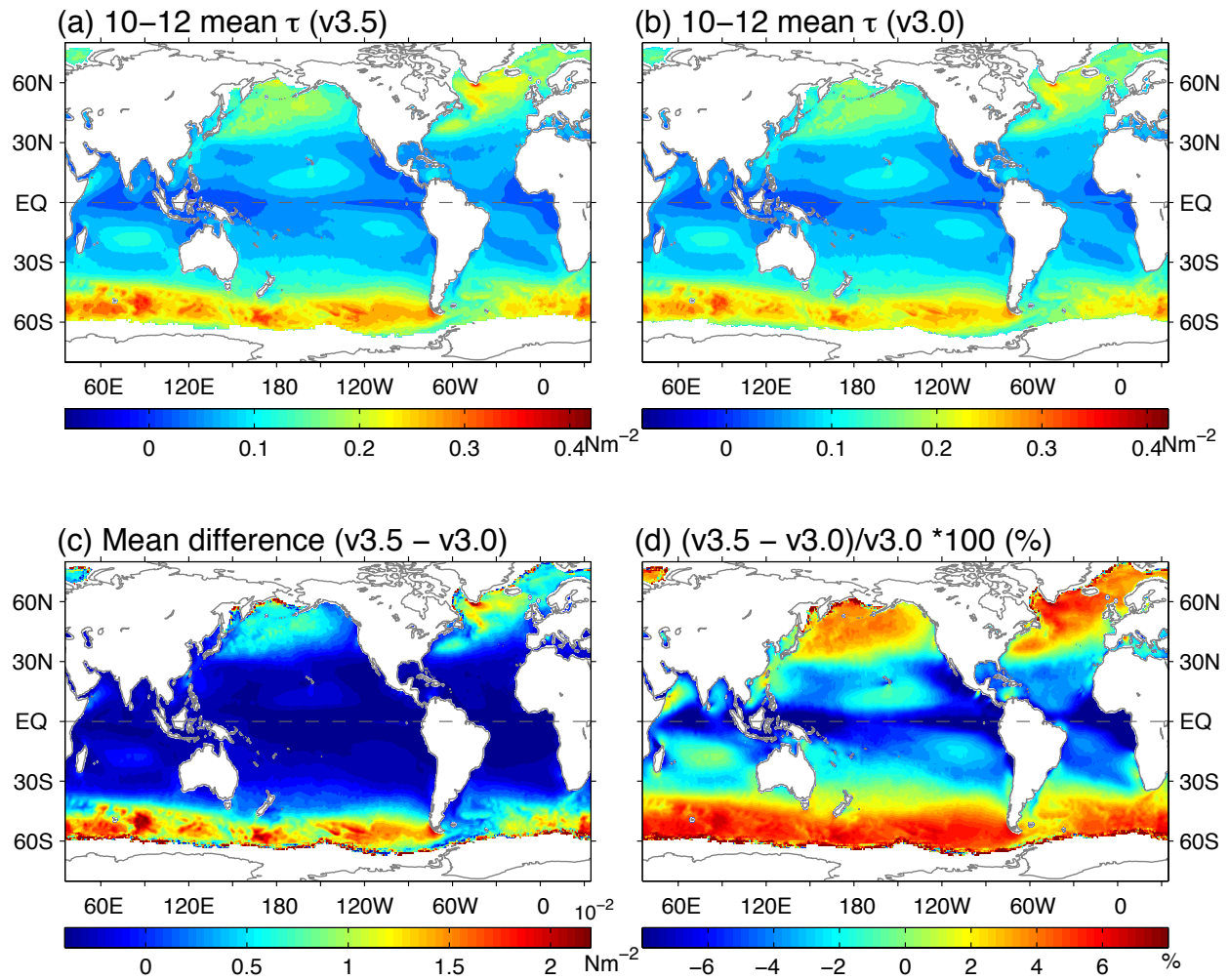


Figure 18. Wind stress computed from (a) COARE v3.5, (b) COARE v3.0. (c) the differences between (a) and (b), and (d) the percentage of the differences. The three-year (2010-2012) mean averages were used as an example.

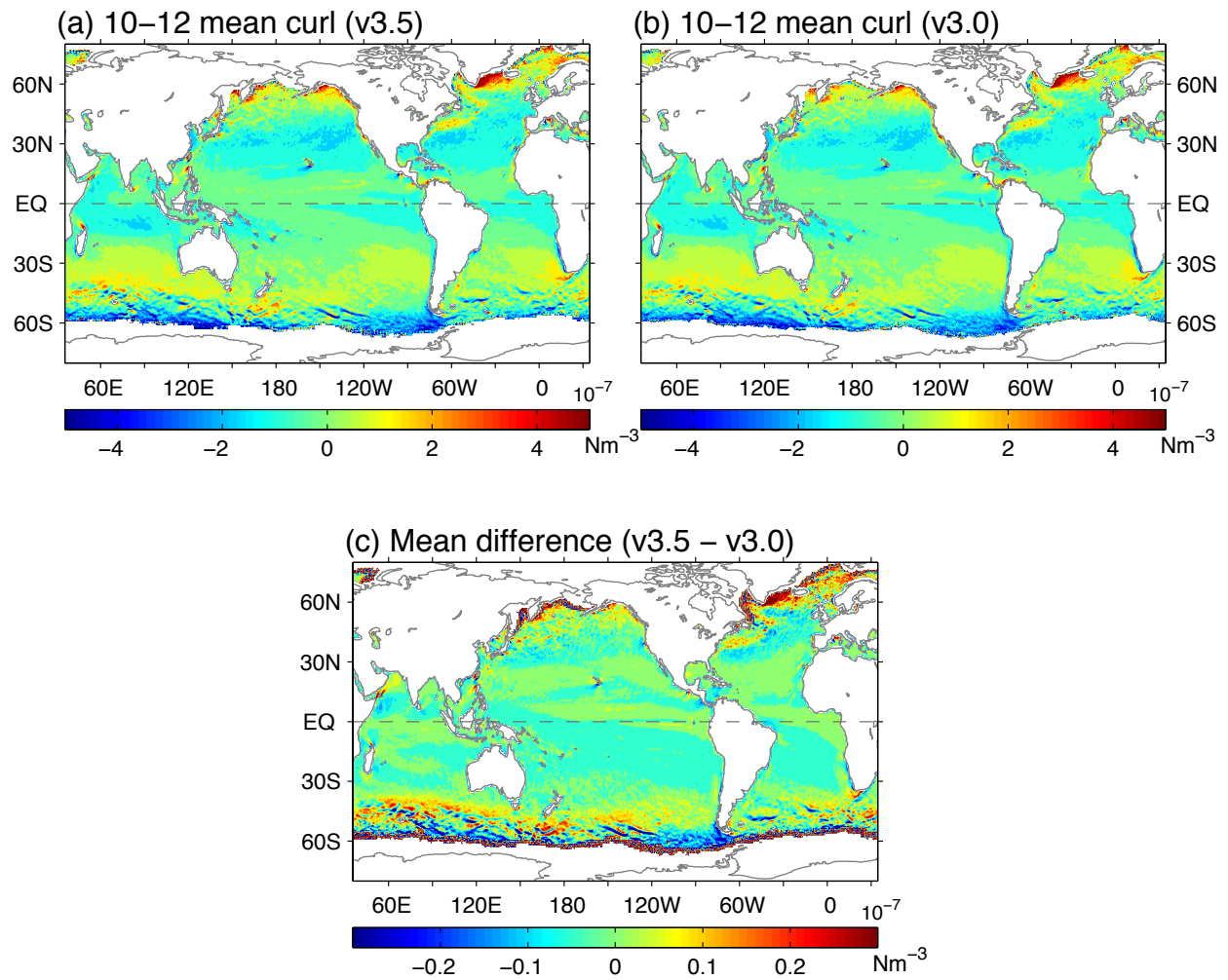


Figure 19. Wind stress curl computed from (a) COARE v3.5, (b) COARE v3.0, and (c) the differences between (a) and (b). The three-year (2010-2012) mean averages were used as an example.

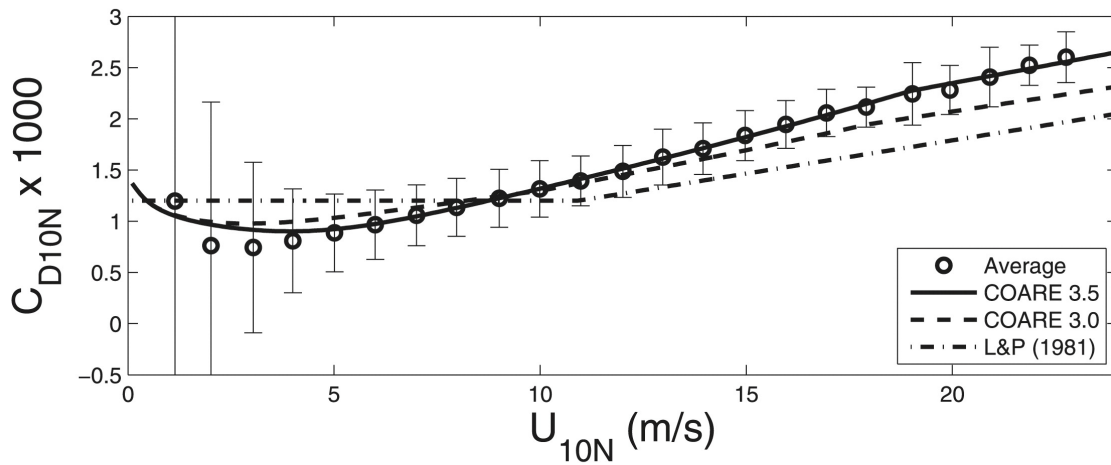


Figure 20. The bin-averaged drag coefficients versus wind speed where the error bars represent the standard deviation about the mean. The dashed line represents the COARE 3.0 algorithm, while the solid line is the COARE 3.5 algorithm. The dashed–dotted line is the function provided by Large and Pond (1981) (from Figure 6 in Edson et al. [2013]).

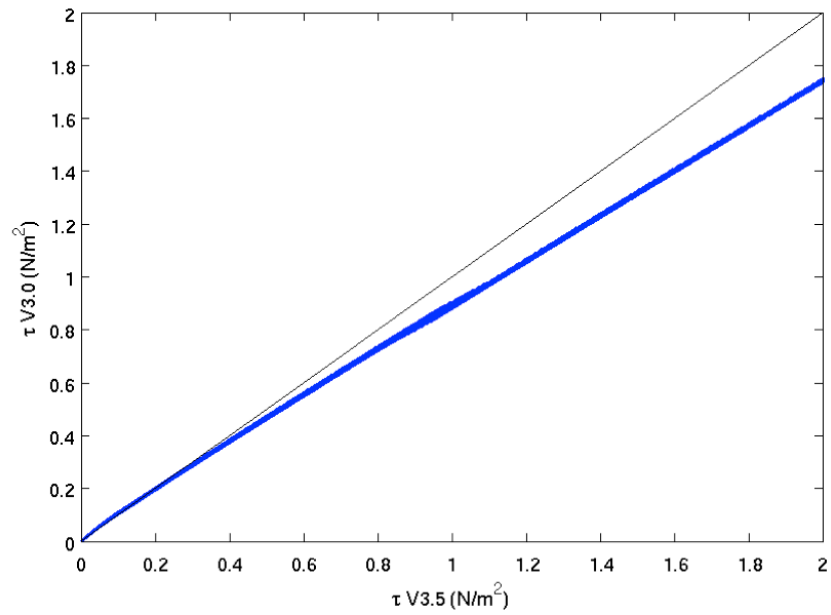


Figure 21. Scatter plot of COARE v3.5 wind stresses (x-axis) versus COARE 3.0 wind stressed (y-axis). The plot was constructed from daily values from all ocean grid points in year 2010.